

Dynamic modulated single-photon routing

Hao-Zhen Li(李浩珍), Ran Zeng(曾然), Miao Hu(胡淼), Mengmeng Xu(许蒙蒙), Xue-Fang Zhou(周雪芳), Xiuwen Xia(夏秀文), Jing-Ping Xu(许静平), and Ya-Ping Yang(羊亚平)
Citation: Chin. Phys. B, 2023, 32 (**12**): 124203. DOI: 10.1088/1674-1056/acf662
Journal homepage: http://cpb.iphy.ac.cn; http://iopscience.iop.org/cpb

What follows is a list of articles you may be interested in

Principle of subtraction ghost imaging in scattering medium

Qin Fu(付芹), Yanfeng Bai(白艳锋), Wei Tan(谭威), Xianwei Huang(黄贤伟), Suqin Nan(南苏琴), and Xiquan Fu(傅喜泉)
Chin. Phys. B, 2023, 32 (**6**): 064203. DOI: 10.1088/1674-1056/acb202

Tunable magnomechanically induced transparency and fast-slow light in a hybrid cavity magnomechanical system

Qinghong Liao(廖庆洪), Kun Peng(彭坤), and Haiyan Qiu(邱海燕)
Chin. Phys. B, 2023, 32 (**5**): 054205. DOI: 10.1088/1674-1056/acaf2b

Tunable phonon-atom interaction in a hybrid optomechanical system

Yao Li(李耀), Chuang Li(李闯), Jiandong Zhang(张建东), Ying Dong(董莹), and Huizhu Hu(胡慧珠)
Chin. Phys. B, 2023, 32 (**4**): 044213. DOI: 10.1088/1674-1056/acb9ea

Effective dynamics and quantum state engineering by periodic kicks

Zhi-Cheng Shi(施志成), Zhen Chen(陈阵), Jian-Hui Wang(王建辉), Yan Xia(夏岩), and X X Yi(衣学喜)
Chin. Phys. B, 2023, 32 (**4**): 044210. DOI: 10.1088/1674-1056/ac7bfc

Ghost imaging based on the control of light source bandwidth

Zhao-Qi Liu(刘兆骐), Yan-Feng Bai(白艳锋), Xuan-Peng-Fan Zou(邹璇彭凡), Li-Yu Zhou(周立宇), Qin Fu(付芹), and Xi-Quan Fu(傅喜泉)
Chin. Phys. B, 2023, 32 (**3**): 034210. DOI: 10.1088/1674-1056/ac6edd

---

Dynamic modulated single-photon routing

Hao-Zhen Li(李浩珍)[1,2,3], Ran Zeng(曾然)[1,†], Miao Hu(胡淼)[1,‡], Mengmeng Xu(许蒙蒙)[1], Xue-Fang Zhou(周雪芳)[1], Xiuwen Xia(夏秀文)[4], Jing-Ping Xu(许静平)[3], and Ya-Ping Yang(羊亚平)[3]

[1] *School of Communication Engineering, Hangzhou Dianzi University, Hangzhou* 310018, *China*
[2] *Zhejiang Province Key Laboratory of Quantum Technology and Device, Zhejiang University, Hangzhou* 310027, *China*
[3] *Key Laboratory of Advanced Micro-Structured Materials of Ministry of Education, School of Physics Science and Engineering, Tongji University, Shanghai* 200092, *China*
[4] *Institute of Atomic and Molecular Physics and Functional Materials, School of Mathematics and Physics, Jinggangshan University, Ji'an* 343009, *China*

(Received 25 July 2023; revised manuscript received 3 September 2023; accepted manuscript online 4 September 2023)

The dynamic control of single-photon scattering in a pair of one-dimensional waveguides mediated by a time-modulated atom–cavity system is investigated. Two cases, where the waveguides are coupled symmetrically or asymmetrically to the atom–cavity system, are discussed in detail. The results show that such time-modulated atom–cavity configuration can behave as a dynamical tunable directional single-photon router. The photons with different frequencies can dynamically be routed from the incident waveguide into any ports of the other with a 100% probability via adjusting the modulated amplitude or phases of the time-modulated atom–cavity coupling strengths, associate with the help of the asymmetrical waveguide–cavity couplings. Furthermore, the influence of dissipation on the routing capability is investigated. It is shown that the present single-photon router is robust against the dissipative process of the system, especially the atomic dissipation. These results are expected to be applicable in quantum information processing and design quantum devices with dynamical modulation.

Keywords: single-photon router, dynamical modulation, waveguide-QED

PACS: 42.50.–p, 42.50.Pq, 03.65.–w **DOI:** 10.1088/1674-1056/acf662

1. Introduction

Quantum networks,[1] which composed of various nodes and channels for storing, processing and distributing quantum information, have been widely applied to quantum computing, quantum simulation, quantum communication, and fundamental tests of physics in large scale space.[2–6] As one kind of typical node devices, quantum routers are essential elements in quantum networks, which can be exploited to transfer information from its source to different quantum channels. In this regard, a variety of theoretical and experimental efforts have been devoted to the realization and development of single-photon router based on atomic systems,[7–9] whispering-gallery resonators,[10–13] optomechanical systems,[14–17] cavity (circuit) quantum electrodynamics (QED),[18–22] and waveguide-QED systems.[23–37]

However, most of the previous single-photon router can only work well with a high routing efficiency at the resonant or selected frequency point under the condition that all the system dissipations are completely ignored.[38–40] The selected frequency points are usually non-adjustable due to the fact that all the system parameters are constants in previous routing schemes. As a result, once the input frequency is altered to outside the selected region, the whole system needs to be reconfigured. In addition, if the system dissipation is taken into account, the routing scheme becomes considerably imperfect and the routing capability shows a drastic reduction.[41,42] These features restrict the scalability and integration of the previous routers for the realization of quantum networks. Therefore, how to achieve a high efficiency and tunable single-photon router, which can not only be operated well for photons with different frequencies in a wide range but also can effectively against the influence of external dissipation, is highly desirable and vital for practical applications in scalable quantum information processing.

In this paper, we develop a dynamical tunable quantum routing scheme for single photons with different frequencies based on a Floquet atom–cavity system, where time modulated coupling strength are introduced to describe the interactions between the atom and the cavity modes. The results reveal that the Floquet atom–cavity structure can be served as a dynamic modulated quantum router, where the routing ports to which single photons are directed or transferred can be dynamically selected, and the incident single photon can be deterministically routed into any selected ports of the two waveguides by adjusting the modulated parameters of the atom–cavity coupling strengths, associated with the help of the asymmetrical waveguide–cavity couplings. More importantly, such router is efficient for photons with different frequencies due to the reason that the optimal working frequency of the router is dynamically tunable within a wide frequency region. In addi-

†Corresponding author. E-mail: zengran@hdu.edu.cn
‡Corresponding author. E-mail: miao_hu@foxmail.com

© 2023 Chinese Physical Society and IOP Publishing Ltd

tion, the results demonstrate that the present router is robust against the system dissipation, and the time modulation of the atom–cavity interactions protects the routing scheme from atomic and cavity loss. Compared to the purely static routing schemes, the routing capability can be improved by introducing time modulation in the presence of dissipation. Especially, by properly designing and manipulating the system parameters, photons can be redirected from one waveguide to any selected ports of another with a 100% probability (deterministically) even when the atomic dissipation is taken into account. These results should be important and meaningful for designing dynamical modulated photonic devices and the studies on dynamic modulated photonic router for photons with different frequencies will certainly contribute to the realizations of future quantum network communications.

The rest of the paper is organized as follows. In Section 2, we introduce the theoretical model of the Floquet waveguide-QED system and derive the analytical expressions for determining the routing probability with a full quantum mechanical method. In Section 3, we first demonstrate how a tunable photonic router for single photon with different frequencies can be achieved for the case that the Floquet atom–cavity system is symmetrically coupled to the two waveguides. Subsequently, we proceed to explore the routing properties with asymmetrical waveguide–cavity couplings. Then, the influence of the system dissipation on the routing capability is discussed, and a brief remark on the experimental feasibility is given. Finally, a conclusion is drawn in Section 4.

2. Model and basic theory

The model under consideration is composed of a pair of parallel one-dimensional waveguides, a two-level atom and two single mode cavities, as schematically shown in Fig. 1. The two waveguides [waveguide M (WM) and waveguide N (WN)] are side coupled to the two cavity modes A and B located at $x=0$ with coupling strengths $V_{d,p}$, $(d=R,L;\ p=m,n)$, respectively. Furthermore, the atom simultaneously couples to the two cavity modes with a periodically modulated coupling strength $g_j(t)=g_0+2\eta\cos(\nu_d t+\phi_j)$, $(j=a,b)$, wherein η the modulated amplitude, ν_d the modulated frequency, ϕ_j the modulated phase and g_0 the static coupling strength.

The total Hamiltonian of the compound system under investigation can be decomposed into three parts as, i.e., $H=H_{\rm free}+H_{\rm wc}+H_{\rm ca}$. The first part is ($\hbar=1$ in what follows)

$$\begin{aligned}H_{\rm free} =& -{\rm i}\upsilon_{\rm g}\sum_{p=m,n}\int {\rm d}x c_{Rp}^{\dagger}(x)\frac{\partial}{\partial x}c_{Rp}(x)\\&+{\rm i}\upsilon_{\rm g}\sum_{p=m,n}\int {\rm d}x c_{Lp}^{\dagger}(x)\frac{\partial}{\partial x}c_{Lp}(x)\\&+(\omega_a-{\rm i}\gamma_a/2)a^{\dagger}a+(\omega_b-{\rm i}\gamma_b/2)b^{\dagger}b\\&+(\omega_{\rm e}-{\rm i}\gamma_{\rm e}/2)\sigma_{ee}+\omega_{\rm g}\sigma_{gg},\end{aligned}\tag{1}$$

which describes the free Hamiltonian of the waveguide photons, the two cavity modes and the atom in the real space. Here, $c_{Rp}^{\dagger}(x)$ $[c_{Lp}^{\dagger}(x)]$ is the creation operator for a right-moving (left-moving) photon along WM $(p=m)$ or WN $(p=n)$ at position x. $\upsilon_{\rm g}$ is the group velocity of the traveling photons in the two waveguides. $c^{\dagger}$ and c $(c=a,b)$ denote the bosonic creation and annihilation operators of the two cavity modes with frequency ω_a and ω_b, respectively. $\omega_{\rm e}$ $(\omega_{\rm g})$ is the eigenfrequency of the atomic excited (ground) state $|e\rangle$ $(|g\rangle)$, and $\sigma_{ee}=|e\rangle\langle e|$, $\sigma_{gg}=|g\rangle\langle g|$. γ_j $(j=a,b,e)$ is the phenomenologically added energy loss rate from the atom or cavities to the free space.

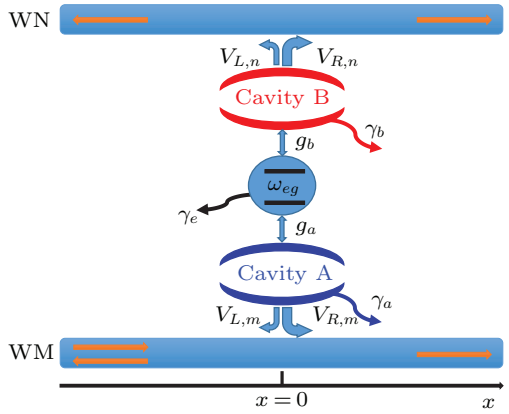


Fig. 1. Schematic diagram of single-photon routing between a pair of one-dimensional waveguides, waveguide M (WM) and waveguide N (WN). Each waveguide couples to the Floquet quantum emitter at $x=0$ with coupling strengths $V_{d,p}$, $(d=R,L;p=m,n)$. The emitter contains a two-level atom (with transition frequency ω_{eg}) and two single mode cavities (denoted by cavity A and cavity B), wherein the two cavity modes couple to the atom with a time modulated coupling strength $g_{j=a,b}$. $\gamma_{a,b}$ and $\gamma_{\rm e}$ denote the decay rates of the cavity modes and the atom, respectively.

The second part $H_{\rm wc}$ of the Hamiltonian H refers to the interactions between the waveguides and cavity modes, which can be expressed as,

$$\begin{aligned}H_{\rm wc} =& \sum_{d=R,L}\int {\rm d}x\delta(x)V_{d,m}c_{dm}^{\dagger}(x)a\\&+\sum_{d=R,L}\int {\rm d}x\delta(x)V_{d,n}c_{dn}^{\dagger}(x)b+{\rm H.c.},\end{aligned}\tag{2}$$

where H.c. denotes the Hermitian conjugate. The third part $H_{\rm ca}$ of the Hamiltonian denote the coupling between the atom and two cavity modes, which takes the form,

$$H_{\rm ca}=g_a(t)a^{\dagger}\sigma_{ge}+g_b(t)b^{\dagger}\sigma_{ge}+{\rm H.c.},\tag{3}$$

here $\sigma_{ge}=|g\rangle\langle e|$ $(\sigma_{eg}=|e\rangle\langle g|)$ is the atomic lowering (raising) ladder operator. By substituting $g_j(t)$ into Eq. (3), the effective Floquet Hamiltonian between the atom and the two cavity modes can be obtained by the standard second-order perturbation as,[43–47]

$$\begin{aligned}H_{\rm ca}^{\rm eff} =& g_0\left(a^{\dagger}\sigma_{ge}+\sigma_{eg}a\right)+g_0\left(b^{\dagger}\sigma_{ge}+\sigma_{eg}b\right)\\&+{\rm i}J_{\rm eff}\left(\sigma_{ee}-\sigma_{gg}\right)\left(b^{\dagger}a-a^{\dagger}b\right),\end{aligned}\tag{4}$$

where $J_{\rm eff} = 2\eta^2 \sin(\phi_a - \phi_b)/v_d$ is the effective coupling strength between the two cavity modes. As a result, the Hamiltonian of the whole system becomes $H_{\rm eff} = H_{\rm free} + H_{\rm wc} + H_{\rm ca}^{\rm eff}$.

Suppose that initially the cavities were empty and the two-level atom was in the ground state. Thus, the scattering eigenstate for the Hamiltonian $H_{\rm eff}$ can be expressed as

$$\begin{aligned}|\Psi\rangle = & \int {\rm d}x\phi_{rm}(x)\, c_{Rm}^{\dagger}(x)\,|v\rangle + \int {\rm d}x\phi_{rn}(x)\, c_{Rn}^{\dagger}(x)\,|v\rangle \\ & + \int {\rm d}x\phi_{lm}(x)\, c_{Lm}^{\dagger}(x)\,|v\rangle + \int {\rm d}x\phi_{ln}(x)\, c_{Ln}^{\dagger}(x)\,|v\rangle \\ & + \mu_a a^{\dagger}|v\rangle + \mu_b b^{\dagger}|v\rangle + \mu_{\rm e}\sigma_{eg}|v\rangle, \end{aligned} \tag{5}$$

where $\phi_{rm}(x)$, $\phi_{rn}(x)$, $\phi_{lm}(x)$, and $\phi_{ln}(x)$ denote the probability amplitudes of the right or left propagating photon in WM or WN. μ_a, μ_b, and $\mu_{\rm e}$ are the excitation amplitudes of cavity A, cavity B, and the atom, respectively. $|v\rangle$ is the vacuum state, which means that no photon in the waveguide or cavities and the atom in ground state $|g\rangle$. If the single photon with frequency ω is injected from the left of WM, then the coefficients $\phi_{rm}(x)$, $\phi_{rn}(x)$, $\phi_{lm}(x)$, and $\phi_{ln}(x)$ in Eq. (5) can be expressed as[41]

$$\begin{aligned}\phi_{rm}(x) &= {\rm e}^{{\rm i}k_m x}[s(-x) + t_m s(x)], \\ \phi_{rn}(x) &= {\rm e}^{{\rm i}k_n x} t_n s(x), \\ \phi_{lm}(x) &= {\rm e}^{-{\rm i}k_m x} r_m s(-x), \\ \phi_{ln}(x) &= {\rm e}^{-{\rm i}k_n x} r_n s(-x), \end{aligned} \tag{6}$$

where $k_{p=m,n} = \omega/v_{\rm g}$, $s(x)$ is the step function with $s(0) = 1/2$. t_m (t_n) denotes the single-photon transmission amplitude and r_m (r_n) represents the reflection amplitude in WM (WN), respectively. By solving the Schrödinger equation $H_{\rm eff}|\Psi\rangle = (\omega + \omega_{\rm g})|\Psi\rangle$,[47,48] one can obtain

$$t_m = \frac{J_{\rm eff}^2 k_{\rm e} + g_0^2(k_a + k_b + {\rm i}\tilde{\Gamma}_m + {\rm i}\Gamma_n) - k_{\rm e}(k_a + {\rm i}\tilde{\Gamma}_m)(k_b + {\rm i}\Gamma_n)}{J_{\rm eff}^2 k_{\rm e} + g_0^2(k_a + k_b + {\rm i}\Gamma_m + {\rm i}\Gamma_n) - k_{\rm e}(k_a + {\rm i}\Gamma_m)(k_b + {\rm i}\Gamma_n)}, \tag{7}$$

$$t_n = \frac{{\rm i}\sqrt{\Gamma_{Rm}\Gamma_{Rn}}(g_0^2 - {\rm i}J_{\rm eff}k_{\rm e})}{J_{\rm eff}^2 k_{\rm e} + g_0^2(k_a + k_b + {\rm i}\Gamma_m + {\rm i}\Gamma_n) - k_{\rm e}(k_a + {\rm i}\Gamma_m)(k_b + {\rm i}\Gamma_n)}, \tag{8}$$

$$r_m = -\frac{{\rm i}\sqrt{\Gamma_{Rm}\Gamma_{Lm}}(g_0^2 - k_b k_{\rm e} - {\rm i}\Gamma_n k_{\rm e})}{J_{\rm eff}^2 k_{\rm e} + g_0^2(k_a + k_b + {\rm i}\Gamma_m + {\rm i}\Gamma_n) - k_{\rm e}(k_a + {\rm i}\Gamma_m)(k_b + {\rm i}\Gamma_n)}, \tag{9}$$

$$r_n = \frac{{\rm i}\sqrt{\Gamma_{Rm}\Gamma_{Ln}}(g_0^2 - {\rm i}J_{\rm eff}k_{\rm e})}{J_{\rm eff}^2 k_{\rm e} + g_0^2(k_a + k_b + {\rm i}\Gamma_m + {\rm i}\Gamma_n) - k_{\rm e}(k_a + {\rm i}\Gamma_m)(k_b + {\rm i}\Gamma_n)}, \tag{10}$$

where $\Gamma_{dp} = V_{d,p}^2 v_{\rm g}$, $(d = R,L;\ p = m,n)$ denotes the corresponding coupling loss between cavity modes and waveguides, $\Gamma_m = (\Gamma_{Rm} + \Gamma_{Lm})/2$, $\Gamma_n = (\Gamma_{Rn} + \Gamma_{Ln})/2$, $\tilde{\Gamma}_m = (\Gamma_{Lm} - \Gamma_{Rm})/2$. $k_{j=a,b} = (\Delta_j + {\rm i}\gamma_j/2)$, and $k_{\rm e} = (\Delta_{eg} + {\rm i}\gamma_{\rm e}/2)$ with $\Delta_j = \omega - \omega_j (\Delta_{eg} = \omega - \omega_{eg})$ the frequency detuning between the waveguide photons and the cavity modes (atom). In the following discussion, we assume that $\omega_a = \omega_b = \omega_{eg} \equiv \omega_0$, correspond to $\Delta_a = \Delta_b = \Delta_{eg} \equiv \Delta$. Furthermore, in order to quantitatively analyze the single photon scattering properties in the waveguides, we introduce the dimensionless quantity $T_m = |t_m|^2$, $T_n = |t_n|^2$, $R_m = |r_m|^2$, and $R_n = |r_n|^2$ for describing the photon transport probability of each ports in WM and WN with $T_m + R_m + T_n + R_n = 1$.

3. Results and discussion

3.1. Routing with symmetrical waveguide–cavity coupling

In this part, we focus on exploring how the photon scattering process can be controlled for the situation that the Floquet atom–cavity system is symmetrically coupled to the two waveguides, i.e., $\Gamma_{Rm} = \Gamma_{Lm} = \Gamma_{Rn} = \Gamma_{Ln} \equiv \Gamma$, and show how a dynamical tunable router for single photons with different frequencies could be implemented by the time modulation.

First, we study how the behaviors of the photon transmission are influenced by the relative modulated phase $\Delta\phi$ for a given modulated amplitude $\eta = 200\Gamma$. In Fig. 2, we plot the transport probabilities $T_{m,n}$ and $R_{m,n}$ as a function of the frequency detuning Δ/Γ for different parameter sets of $\Delta\phi = \phi_a - \phi_b$ and the static atom–cavity coupling strength g_0. One can find that the transport of the incident photon can be effectively controlled by $\Delta\phi$, and the system can behave as a phase-modulated single photon router. Specifically, for the case of $g_0 = 0$ and $\Delta\phi = 0$ (corresponding to $J_{\rm eff} = 2\eta^2 \sin(\phi_a - \phi_b)/v_d = 0$), both the effective coupling between atom–cavity and two cavity modes vanish, which means that the whole compound system is degenerated to a single waveguide side coupled by an optical cavity. In this case, the transmission spectrum of photons in the incident waveguide displays a Lorentzian or inverted Lorentzian line shape with $T_m = 0$ and $R_m = 1$ at the resonant point due to the perfect destructive interference between the incident wave and the re-emitted one [see the red solid and blue dash line in Fig. 2(a)], and the incoming single photon cannot be transferred into the other waveguide with $T_n = 0$ and $R_n = 0$, as shown by the green dot and cyan dashed-dot line in Fig. 2(a).

However, if we modulate the two coupling strengths g_a and g_b out of phase, i.e., $g_0 = 0$ and $\Delta\phi = \pi/2$, the Floquet atom–cavity system can be treated as two coupled optical cav-

ities. In this case, the effective coupling between the two cavity modes becomes nonzero, i.e., $J_{\rm eff} = 8\Gamma$, which leads to the normal mode splitting with $\Delta = \pm J_{\rm eff}$. As a result, an incident single photon with frequency $\omega = \omega_0 \pm J_{\rm eff}$ can be absorbed by the coupled cavity system and then re-emitted into arbitrary output ports of either the incident waveguide or the other one with the same probability [as shown in Fig. 2(b)], which indicates that the considered Floquet atom–cavity system can work as a single photon router for routing the photon to either of the two waveguides. Interestingly, comparing Figs. 2(a) and 2(b), one can find that such the photon routing is phase-sensitive. The single photon routing between the two waveguides can be controlled by tuning the modulated phases of the two atom–cavity coupling strengths.

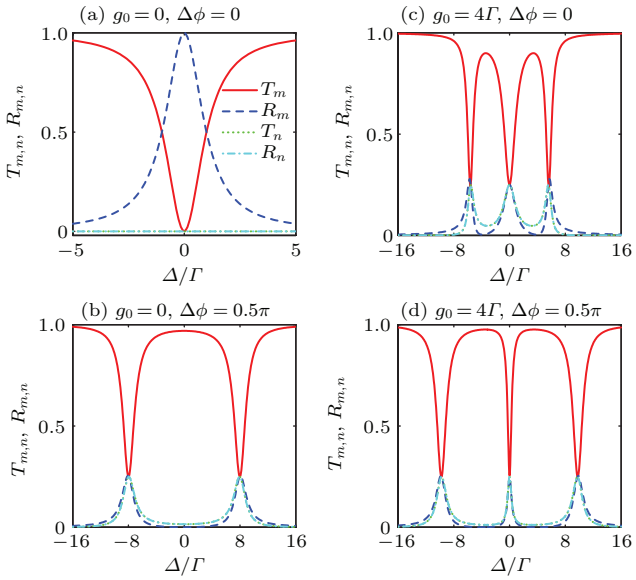


Fig. 2. The transport probabilities T_m, T_n, R_m, and R_n as a function of the frequency detuning Δ/Γ for different parameter sets of $\Delta\phi$ and g_0. The other common parameters are $\eta = 200\Gamma$, $\nu_d = 50\eta$, and $\gamma_e = \gamma_a = \gamma_b = 0$, respectively.

In Figs. 2(c) and 2(d), we further demonstrating the phase modulated single photon routing by taking into account the static atom–cavity coupling with $g_0 \neq 0$. It is found that the transfer spectra (denoted by the green dot and cyan dashed-dot line) display three transfer peaks (a resonant peak and two symmetric sideband peaks) due to the vacuum Rabi splitting[49] combined with the normal mode splitting, which originating from the effective interaction between the atom–cavity and the two cavity modes. The three transfer peaks located at $\Delta = 0$ and $\Delta = \pm\sqrt{J_{\rm eff}^2 + 2g_0^2}$ corresponding to three optimal routing windows for photons with different frequencies. It can be seen that either resonant photon or non-resonant photons with frequency around the two sideband optimal routing windows can effectively be routed from the incident waveguide to the other one. Furthermore, it should be pointed out that the locations of the two sideband optimal routing windows are phase-dependent due to the fact that the effective coupling strength $J_{\rm eff} = 2\eta^2 \sin\Delta\phi/\nu_d$ is determined by $\Delta\phi$. This means that, by altering the relative modulated phase, one can dynamically tune the frequency values where optimal routing is attained.

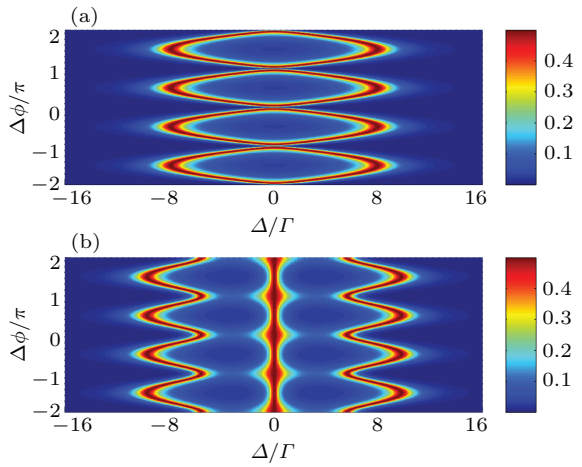


Fig. 3. The contour map of the transfer probability $P_n = T_n + R_n$ as a function of both Δ/Γ and $\Delta\phi$ with $g_0 = 0$ in panel (a) and $g_0 = 4\Gamma$ in panel (b). Other common parameters are the same as those shown in Fig. 2.

This remarkable feature can be further demonstrated in Fig. 3, where the variations of P_n ($P_n = T_n + R_n$ denotes the transfer probability of the single photon from WM to WN) versus both Δ/Γ and $\Delta\phi$ with $g_0 = 0$ and $g_0 = 4\Gamma$ are plotted in Figs. 3(a) and 3(b), respectively. It is shown that, there are two bright red oscillate zones in both cases, which corresponding to the two sideband optimal routing windows discussed above. Obviously, the frequency (or location) of each sideband optimal routing windows is a periodic function of the relative modulated phase $\Delta\phi$. Within a period, the optimal frequency point can be tuned from $\Delta = 0$ ($\Delta = \pm\sqrt{2}g_0$) to $\Delta = \pm J_{\rm eff}$ ($\Delta = \pm\sqrt{J_{\rm eff}^2 + 2g_0^2}$) by increasing $\Delta\phi$ from 0 to $\pi/2$ for the case of $g_0 = 0$ ($g_0 = 4\Gamma$). This means that an incident single photon with frequency within these optimal frequency regions can be dynamically routed into WN via adjusting the relative modulated phase, which also implies that a dynamic modulated router for single photon with different frequencies can be realized. It is worth indicating that such dynamic modulated single photon router can also be implemented by tuning the modulated amplitude η, and the optimal frequency regimes can further be enlarged via increasing η due to the relationship $\Delta = \pm\sqrt{J_{\rm eff}^2 + 2g_0^2}$ with $J_{\rm eff} = 2\eta^2 \sin\Delta\phi/\nu_d$.

Below, we explore how to control the single photon routing between the two waveguides through varying the modulated amplitude η for a given relative modulated phase $\Delta\phi = \pi/2$. The transfer probability P_n versus both Δ/Γ and η are plotted in Fig. 4(a) with $g_0 = 0$ and in Fig. 4(b) with $g_0 = 4\Gamma$, respectively. It is obvious from Fig. 4 that the transfer spectra are strongly related to η. For the case of $g_0 = 0$, when η is very small ($J_{\rm eff} = 2\eta^2 \sin\Delta\phi/\nu_d \approx 0$), the two cavity modes are decoupled. As a result, no photon can be routed from WM into WN, which is consistent with that discussed in Fig. 2(a). With

η gradually increasing, $J_{\rm eff}$ becomes nonzero, which plays an essential role in the spectral line shapes and a normal mode splitting with $\Delta = \pm J_{\rm eff}$ can be observed, as shown by the two bright red zones in Fig. 4(a). The width between the two red zones increases with the increasing of η. According to what discussed in Figs. 2 and 3, this suggests that the optimal routing frequency regime can be further enlarged depending on η.

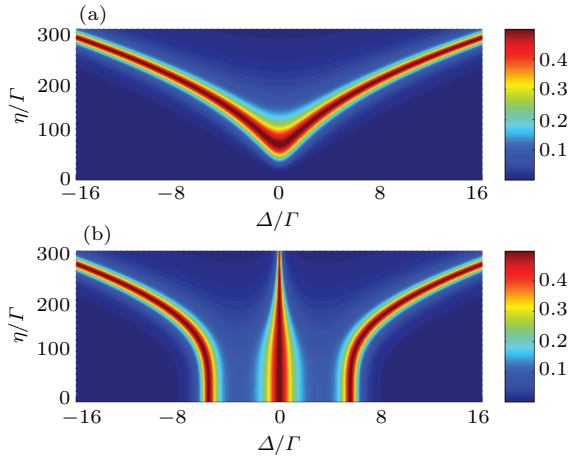


Fig. 4. The contour map of the transfer probability $P_n = T_n + R_n$ as a function of both Δ/Γ and η/Γ with $g_0 = 0$ in panel (a) and $g_0 = 4\Gamma$ in panel (b). Other common parameters are the same as those shown in Fig. 2, except that $\Delta\phi = \pi/2$.

For the case of $g_0 = 4\Gamma$, a similar result can be obtained. When η is extremely weak ($J_{\rm eff} \approx 0$), the composite Floquet quantum structure is equivalently reduced back to a purely static atom–cavity system. As a result, both the transfer probability and the location of the two sideband optimal routing windows are insensitive to the modulated amplitude. However, by increasing η gradually, a larger optimal routing frequency region can be obtained according to $\Delta = \pm\sqrt{J_{\rm eff}^2 + 2g_0^2}$, as shown by the bright red zones in Fig. 4(b). Consequently, a dynamic modulated router, which is efficient for photons within a large frequency region, can also be implemented by carefully manipulating the modulated amplitude η.

3.2. Routing with asymmetrical waveguide–cavity coupling

In previous part, we demonstrated a tunable photonic router for single photon with different frequencies via dynamically modulating the coupling strengths between the atom and the two cavity modes. However, the routing efficiency between the waveguides is extremely limited to no more than 50% due to the symmetrical coupling, i.e., $\Gamma_{Rm} = \Gamma_{Lm} = \Gamma_{Rn} = \Gamma_{Ln} \equiv \Gamma$. As we know, a reliable photonic routing scheme is required to be not only controllable but also able to redirect photons with high routing efficiency. In order to improve the routing capability, asymmetrical waveguide–cavity couplings, i.e., $\Gamma_{Rm} \neq \Gamma_{Lm}$, $\Gamma_{Rn} \neq \Gamma_{Ln}$, are considered below.

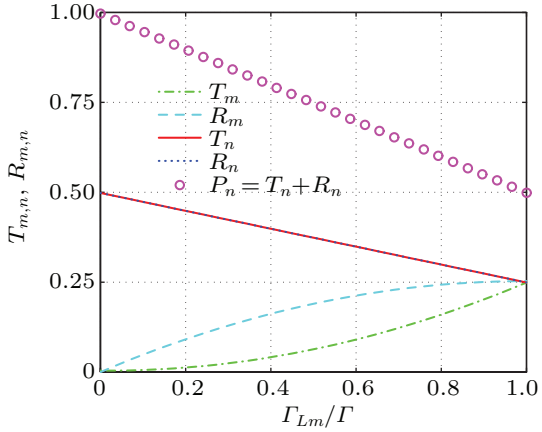


Fig. 5. The transport probabilities $T_{m,n}$, $R_{m,n}$, and P_n as a function of Γ_{Lm}/Γ with $\Gamma_{Ln} = \Gamma_{Rn}$, $\Delta = 8J_{\rm eff}$, $\Delta\phi = \pi/2$, and $g_0 = 0$. Other common parameters are the same as those shown in Fig. 2.

In Fig. 5, the transport probabilities $T_{m,n}$, $R_{m,n}$, and P_n of routing the input photon with frequency $\Delta = 8J_{\rm eff}$ to various output ports versus Γ_{Lm}/Γ with fixed modulated parameters under the condition $\Gamma_{Ln} = \Gamma_{Rn}$ are plotted. It can be seen that, comparing to the symmetrical case where $T_m = R_m = T_n = R_n = 0.25$ at the frequency point $\Delta = 8J_{\rm eff}$, T_m, $R_m < 0.25$, and $T_n = R_n > 0.25$ can be obtained by decreasing Γ_{Lm} in the region $\Gamma_{Lm} < \Gamma$. In the ideal case, i.e., $\Gamma_{Lm} = 0$, the transfer rate P_n reaches its maximum 1 (see the pink circle) with $T_m = R_m = 0$ and $T_n = R_n = 0.5$. This means that the incident single photon from WM can be completely routed into WN but symmetrically output either from the left or right port with equal probability. To deterministically route the single photon into the two output ports, we can further break the symmetry between Γ_{Ln} and Γ_{Rn}.

In Fig. 6, the transport probabilities T_n and R_n versus both Γ_{Ln}/Γ and Γ_{Rn}/Γ are plotted in Figs. 6(a) and 6(b), respectively. It can be seen that T_n (R_n) can be further enhanced to $T_n > 0.5$ ($R_n > 0.5$) at the expense of decreasing R_n (T_n) below 0.5 under the condition $\Gamma_{Rn} > \Gamma_{Ln}$ ($\Gamma_{Rn} < \Gamma_{Ln}$). This is because the asymmetrical coupling, i.e., $\Gamma_{Ln} \neq \Gamma_{Rn}$, leads to an imbalance between the reemitting photons to the left and right directions of WN. In the ideal case, i.e., $\Gamma_{Ln} = 0$, $\Gamma_{Rn} = 2\Gamma$ or $\Gamma_{Ln} = 2\Gamma$, $\Gamma_{Rn} = 0$, the incident single photon can be fully redirected into the right or left port of WN with $T_n \approx 1$ or $R_n \approx 1$, as shown by the bright red zones in Figs. 6(a) and 6(b). These results clearly show that the present proposed routing scheme can transfer photons from the input port to other arbitrarily selected one with a perfect transfer efficiency. This also implies that a dynamical tunable targeted single-photon router with 100% routing probability can be achieved with the help of the asymmetric waveguide–cavity coupling. For further insight, the transport probabilities versus the dynamical modulating parameters, i.e., $\Delta\phi$ and η, under the asymmetrical conditions are given in Figs. 7 and 8, respectively.

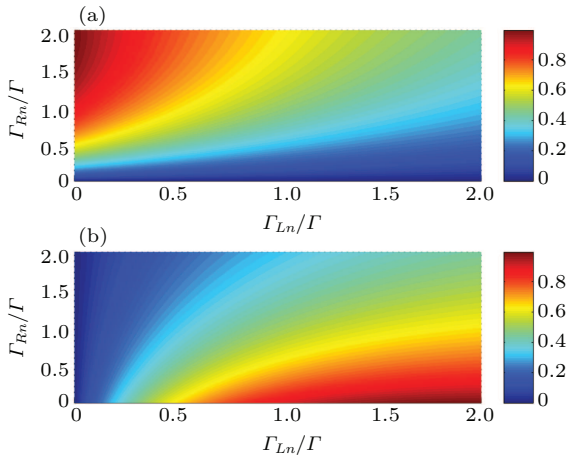


Fig. 6. The contour map of the transport probability T_n (a) and R_n (b) as a function of both Γ_{Ln}/Γ and Γ_{Rn}/Γ with $\Gamma_{Lm}=0$, $\Gamma_{Rm}=2\Gamma$. Other common parameters are the same as those shown in Fig. 5.

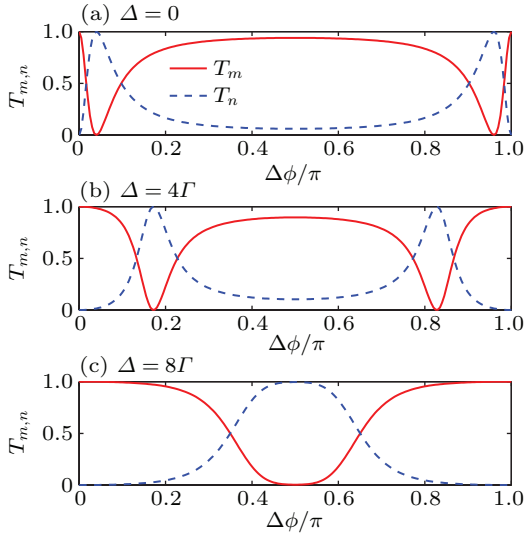


Fig. 7. The transport probability T_n and T_m as a function of $\Delta\phi$ for different photon frequencies with $\Delta=0$, 4Γ, 8Γ in panels (a)–(c), respectively. Other common parameters are the same as those shown in Fig. 5, except that $\Gamma_{Lm}=\Gamma_{Ln}=0$, $\Gamma_{Rm}=\Gamma_{Rn}=2\Gamma$.

In Fig. 7, we show how a dynamical tunable targeted single-photon router can be implemented by manipulating the relative modulated phase $\Delta\phi$. Without loss of generality and for simplicity, we assume that $\Gamma_{Lm}=\Gamma_{Ln}=0$ and $\Gamma_{Rm}=\Gamma_{Rn}=2\Gamma$, which means that the incident photon from the input port can only be directed rightwards, and correspondingly both the probability amplitudes R_m and R_n vanish. The transport probabilities T_m and T_n of routing the incident photon to the right ports of WM and WN, with respect to $\Delta\phi$ and different inputting frequencies (i.e., $\Delta=0$, 4Γ, 8Γ), are plotted in Figs. 7(a)–7(c), respectively. It can be seen that, for incident photon with fixed frequencies, the relative phase $\Delta\phi$ plays an important role in manipulating the photon routing. The transport probabilities can be tuned from 0 to 1 by properly adjusting $\Delta\phi$, with the behaviors of T_m and T_n show opposite trends. Namely, when T_n increases to the maximal 1, T_m will decrease to its minimal 0, and *vice versa*. These results indicate that the incident single photon with different frequencies can either be redirected into the right port of WM or WN with a determinately routing probability of 100%. Furthermore, the relative modulated phase can behave as dynamical switch to turn on or off the photon routing between the two desired ports of WM and WN, which implies that a dynamic modulated directional single-photon router can be realized.

In Fig. 8, The transport probabilities T_m and T_n versus the modulated amplitude η with different inputting frequencies (i.e., $\Delta=0$, 4Γ, 8Γ) are plotted. The results show again that both T_n and T_m can be modulated from 0 to 1 with opposite trends, which implies that a dynamical tunable single-photon router between the two desired ports of WM and WN can also be implemented by controlling the modulated amplitude η. We would like to point out that such dynamic modulated directional single-photon router can also be achieved between any other selected output ports of the two waveguides by carefully designing and manipulating the asymmetrical coupling conditions, and such photonic router can also be studied in a similar way as those discussed above when the influence of the static atom–cavity coupling is taken into account (not shown here due to the length limitation).

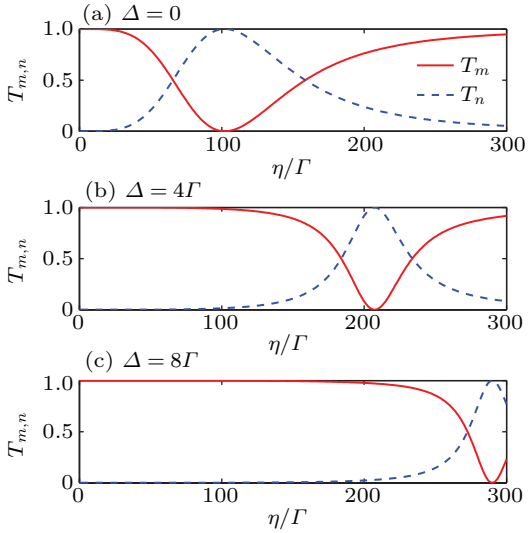


Fig. 8. The transport probability T_n and T_m as a function of η/Γ for different photon frequencies with $\Delta=0$, 4Γ, 8Γ in panels (a)–(c), respectively. Other common parameters are the same as those shown in Fig. 5, except that $\Gamma_{Lm}=\Gamma_{Ln}=0$, $\Gamma_{Rm}=\Gamma_{Rn}=2\Gamma$.

3.3. Influence of dissipation

Up to now, we have demonstrated that how an ideal dynamical tunable single-photon router can be realized and be controlled by the time modulations in the absence of dissipation. However, in any realistic physical system, the effects of dissipation cannot be ignored. In the present system, the main dissipation originates from spontaneous emission of the two-level atom and the intrinsic dissipative process of the two cavity modes. With this concern, in what follows, we focus on exploring how the routing capability is influenced by the atomic and cavity decays.

First, we study how the routing efficiency is affected by the atomic spontaneous emission. The variations of the routing probability T_n versus the frequency detuning Δ/Γ and the atomic decay rate γ_e for different parameter sets of g_0 and η are plotted in Figs. 9(a)–9(c), respectively. It is clear from Fig. 9(a) that, for the case of $g_0 = 4\Gamma$ and $\eta = 0$ [corresponding to the purely static atom–cavity coupling system discussed in Fig. 2(c)], the routing efficiency of both the resonant ($\Delta = 0$) and non-resonant ($\Delta = 5.6\Gamma$) photons decreases with increasing γ_e, but the non-resonant photons are more sensitive to the atomic decay than the resonant one. However, if we dynamically modulating the atom–cavity coupling strengths with $\eta = 200\Gamma$, the behaviors of the sensitivity show opposite trend, *e.g.*, the non-resonant photons become insensitive to γ_e, as shown in Fig. 9(b). More importantly, in this case, the routing efficiency of the non-resonant photons can persist a high value even when the atomic decay rate become large, and this high routing efficiency can be further improved to approach 1 by properly adjusting the static atom–cavity coupling strength, i.e., $g_0 = 0$, as shown in Fig. 9(c). These remarkable results can be seen more clearly in Fig. 9(d), where the routing efficiencies of the non-resonant photons corresponding to each case of Figs. 9(a)–9(c) are plotted. According to Fig. 9, from the routing perspective, one can come to a conclusion that the dynamical interaction between atom and cavity modes protect the present photonic routing scheme from atomic dissipation, although the inputting frequencies are different.

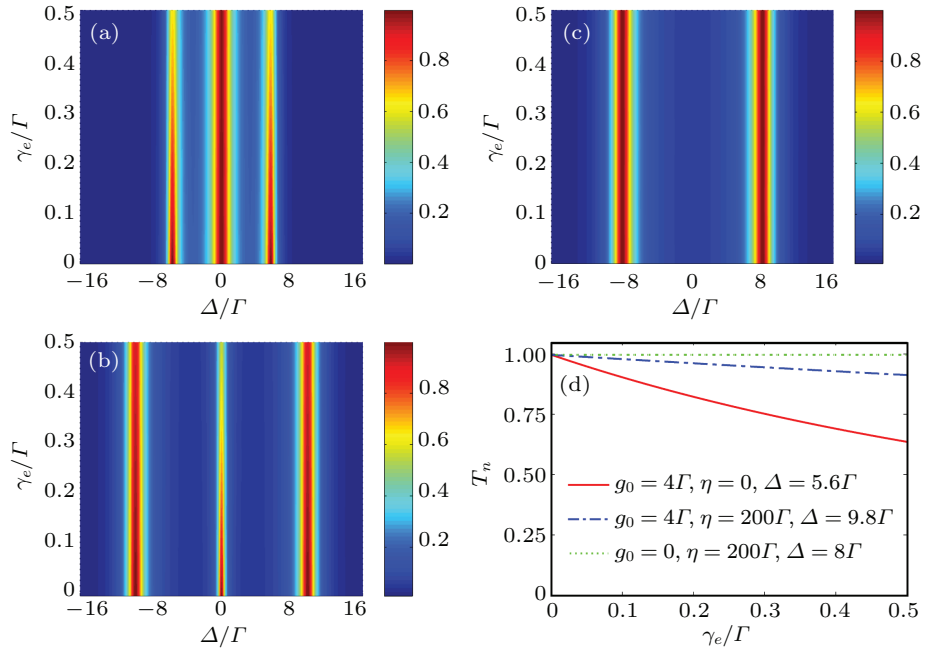


Fig. 9. The contour map of the transport probability T_n as a function of both Δ/Γ and γ_e/Γ for different parameter sets of η and g_0: $\eta = 0$, $g_0 = 4\Gamma$ in panel (a); $\eta = 200\Gamma$, $g_0 = 4\Gamma$ in panel (b); $\eta = 200\Gamma$, $g_0 = 0$ in panel (c). (d) T_n as a function of γ_e/Γ for special parameter sets of η, g_0, and Δ. Other common parameters are $\Delta\phi = \pi/2$, $\nu_d = 50\eta$, $\Gamma_{Lm} = \Gamma_{Ln} = 0$, $\Gamma_{Rm} = \Gamma_{Rn} = 2\Gamma$, and $\gamma_a = \gamma_b = 0$, respectively.

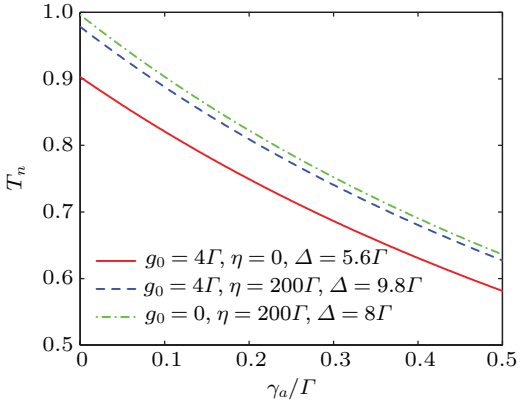


Fig. 10. The transport probability T_n as a function of γ_a/Γ for different parameter sets of η, g_0, and Δ. Other common parameters are the same as those shown in Fig. 9, except that $\gamma_e = 0.1\Gamma$ and $\gamma_b = \gamma_a$.

Then, we proceed to study how the cavity dissipation affects the routing capability. In Fig. 10, the routing efficiency is plotted as a function of the cavity decay rate for three different parameter sets of g_0, η, and Δ. It is shown that, due to the time modulation, the routing scheme can be notably improved even in the presence of cavity loss. All in all, figures 9 and 10 indicate that the quality of such a dynamically modulated single photon router is robust against to the atomic and cavity dissipation.

3.4. Physical implementation

Before summary, let us provide a brief remark on the experimental feasibility of our scheme. As schematically shown in Fig. 1, the present scheme can be implemented in different physical platforms, including superconducting circuits,[50] optomechanical circuits[51] or photonic-crystal resonator lattice.[52] As superconducting circuits for example, the single-mode cavity, the two-level atom and the one-dimensional waveguide can be achieved by a superconducting resonator, a superconducting qubit and a superconducting

transmission line, respectively. In our model, one of the key elements is the time-modulated coupling between the atom and the two cavity modes, which can be realized by embedding a superconducting quantum interference device between the qubit and the two resonators.[53–55] Another one is the chiral interaction between the waveguides and the cavity modes, which can be achieved by inserting circulators in superconducting circuits.[56] Consequently, if the two points can be realized perfectly, then the dynamical tunable directional single-photon router may be demonstrated in a circuit-QED system.

Next, we examine the realistic parameter space for physical implementation under the existing experimental techniques. To simulate the transmission properties of the waveguide photons, all the system parameters are normalized to Γ in the numerical simulation, *e.g.*, the static coupling strength g_0 assumed to be 4Γ. It was demonstrated that the decay rate Γ (corresponding to the coupling between cavity modes and waveguides) can be adjusted from zero to hundreds of megahertz in a circuit QED experiment.[57] Then for a given Γ, *e.g.*, $\Gamma/2\pi = 25$ MHz, one can obtain $g_0/2\pi = 100$ MHz, which is a typical atom–cavity coupling constant attainable with modern circuit-QED technologies.[58,59]

4. Conclusion

In conclusion, we have theoretically studied the coherent scattering process of photons between two one-dimensional waveguides side coupling to a Floquet atom–cavity system, wherein the atom dynamically interacts with the cavity modes with time-modulated coupling strengths. The results indicate that such Floquet atom–cavity system can behave as a dynamical tunable targeted single photon router, which can dynamically route the incident waveguide photon into any ports of the other with a 100% probability via adjusting the modulated parameters introduced into the atom–cavity coupling strengths, associate with the help of the asymmetrical waveguide–cavity couplings. Compared to previous routing schemes, this scheme has following advantages: (i) The application of the dynamical modulated atom–cavity coupling strength instead of a purely static one makes our photonic router more tunable. The optimal working frequency of the router is dynamically tunable within a wide frequency region, which makes this router efficient for photons with different frequencies. (ii) The present router is robust against the system dissipation, and the time modulation of the atom–cavity interactions protects the routing scheme from atomic and cavity loss. Under appropriate conditions, photons can be redirected from one waveguide to any selected ports of another with a 100% probability even in the presence of atomic dissipation. These advantages are expected to be applicable in quantum network communication.

Acknowledgements

Project supported by China Postdoctoral Science Foundation (Grant No. 2023M732028), the Fund from Zhejiang Province Key Laboratory of Quantum Technology and Device (Grant No. 20230201), the Fundamental Research Funds for the Provincial Universities of Zhejiang Province, China (Grant No. GK199900299012-015), the Natural Science Foundation of Zhejiang Province, China (Grant No. LY21A040003), the National Natural Science Foundation of China (Grant Nos. 12164022, 12174288, and 12274326), and the Natural Science Foundation of Jiangxi Province, China (Grant No. 20232BAB201044).

References

[1] Kimble H J 2008 *Nature* **453** 1023
[2] Ritter S, Nölleke C, Hahn C, Reiserer A, Neuzner A, Uphoff M, Mücke M, Figueroa E, Bochmann J and Rempe G 2012 *Nature* **484** 195
[3] Pichler H, Ramos T, Daley A J and Zoller P 2015 *Phys. Rev. A* **91** 042116
[4] Mahmoodian S, Lodahl P and Sørensen A S 2016 *Phys. Rev. Lett.* **117** 240501
[5] Reiserer A and Rempe G 2015 *Rev. Mod. Phys.* **87** 1379
[6] Su K, Wang Y, Zhang S, Kong Z, Zhong Y, Li J, Yan H and Zhu S L 2021 *Chin. Phys. Lett.* **38** 094202
[7] Li X and Wei L F 2015 *Phys. Rev. A* **92** 063836
[8] Zhou L, Yang L P, Li Y and Sun C 2013 *Phys. Rev. Lett.* **111** 103604
[9] Shomroni I, Rosenblum S, Lovsky Y, Bechler O, Guendelman G and Dayan B 2014 *Science* **345** 903
[10] Aoki T, Parkins A S, Alton D J, Regal C A, Dayan B, Ostby E, Vahala K J and Kimble H J 2009 *Phys. Rev. Lett.* **102** 083601
[11] Xia K and Twamley J 2013 *Phys. Rev. X* **3** 031013
[12] Huang J S, Zhang J H and Wei L F 2018 *J. Phys. B: At. Mol. Opt. Phys.* **51** 085501
[13] Cao C, Duan Y W, Chen X, Zhang R, Wang T J and Wang C 2017 *Opt. Express* **25** 16931
[14] Papon C, Zhou X, Thyrrestrup H, Liu Z, Stobbe S, Schott R, Wieck A D, Ludwig A, Lodahl P and Midolo L 2019 *Optica* **6** 524
[15] Agarwal G S and Huang S 2012 *Phys. Rev. A* **85** 021801
[16] Li G, Xiao X, Li Y and Wang X 2018 *Phys. Rev. A* **97** 023801
[17] Fang K, Matheny M H, Luan X and Painter O 2016 *Nat. Photon.* **10** 489
[18] Xia K, Jelezko F and Twamley J 2018 *Phys. Rev. A* **97** 052315
[19] Zhu Y T and Jia W Z 2019 *Phys. Rev. A* **99** 063815
[20] Ren Y L, Ma S L, Xie J K, Li X K, Cao M T and Li F L 2022 *Phys. Rev. A* **105** 013711
[21] Hoi I C, Wilson C M, Johansson G, Palomaki T, Peropadre B and Delsing P 2011 *Phys. Rev. Lett.* **107** 073601
[22] Rosenblum S, Parkins S and Dayan B 2011 *Phys. Rev. A* **84** 033854
[23] Zhang Y Q, Zhu Z H, Chen K K, Peng Z H, Yin W J, Yang Y, Zhao Y Q, Lu Z Y, Chai Y F, Xiong Z Z and Tan L 2022 *Front. Phys.* **10** 1054299
[24] Yan G A and Lu H 2021 *Phys. Scr.* **96** 105102
[25] Lu J, Wang Z and Zhou L 2015 *Opt. Express* **23** 22955
[26] Li X, Xin J, Li G, Lu X M and Wei L F 2021 *Opt. Express* **29** 8861
[27] Wang C, Ma X S and Cheng M T 2021 *Opt. Express* **29** 40116
[28] Lu J, Zhou L, Kuang L M and Nori F 2014 *Phys. Rev. A* **89** 013805
[29] Ahumada M and Orellana P A, Domínguez-Adame F and Malyshev A V 2019 *Phys. Rev. A* **99** 033827
[30] Wu J N, Dong J, Xu Y, Zou B and Zhang Y 2022 *Phys. Rev. Appl.* **18** 054007
[31] Yan W B and Fan H 2015 *Sci. Rep.* **4** 4820
[32] Wang X, Yang W X, Chen A X, Li L, Shui T, Li X and Wu Z 2022 *Quantum Sci. Technol.* **7** 015025
[33] Yang Y, Lu J and Zhou L 2022 *Commun. Theor. Phys.* **74** 025101
[34] Yan G A and Lu H 2022 *Front. Phys.* **10** 880117
[35] Zhang J H, He D Y, Luo G Y, Wang B D and Huang J S 2021 *Chin. Phys. B* **30** 034204
[36] Liu J S, Yang Y, Lu J and Zhou L 2022 *Chin. Phys. B* **31** 110301

[37] Shu Y X, Ma X S, Huang X S, Cheng M T and Han J B 2021 *Chin. Phys. B* **30** 104204
[38] Cheng M T, Ma X S, Zhang J Y and Wang B 2016 *Opt. Express* **24** 19988
[39] Gonzalez-Ballestero C, Moreno E, Garcia-Vidal F J and Gonzalez-Tudela A 2016 *Phys. Rev. A* **94** 063817
[40] Yan C H, Li Y, Yuan H and Wei L 2018 *Phys. Rev. A* **97** 023821
[41] Yang D C, Cheng M T, Ma X S, Xu J, Zhu C and Huang X S 2018 *Phys. Rev. A* **98** 063809
[42] Poudyal B and Mirza I M 2020 *Phys. Rev. Res.* **2** 043048
[43] Li H, Cai H, Xu J, Yakovlev V V, Yang Y and Wang D W 2019 *Opt. Express* **27** 6946
[44] Wang D W, Cai H, Liu R B and Scully M O 2016 *Phys. Rev. Lett.* **116** 220502
[45] Wang D W, Song C, Feng W, Cai H, Xu D, Deng H, Li H, Zheng D, Zhu X, Wang H, Zhu S Y and Scully M O 2019 *Nat. Phys.* **15** 382
[46] Goldman N and Dalibard J 2014 *Phys. Rev. X* **4** 031027
[47] Li H, Li Z, Zeng R, Hu M, Xu M, Zhou X, Xia X, Xu J and Yang Y 2023 *Phys. Rev. A* **107** 023720
[48] Shen J T and Fan S 2009 *Phys. Rev. A* **79** 023837
[49] Yoshie T, Scherer A, Hendrickson J, Khitrova G, Gibbs H M, Rupper G, Ell C, Shchekin O B and Deppe D G 2004 *Nature* **432** 200
[50] Blais A, Huang R S, Wallraff A, Girvin S M and Schoelkopf R J 2004 *Phys. Rev. A* **69** 062320
[51] Fang K, Luo J, Metelmann A, Matheny M H, Marquardt F, Clerk A A and Painter O 2017 *Nat. Phys.* **13** 465
[52] Fang K, Yu Z and Fan S 2012 *Nat. Photon.* **6** 782
[53] Hime T, Reichardt P A, Plourde B L T, Robert-son T L, Wu C E, Ustinov A V and Clarke J 2006 *Science* **314** 1427
[54] Allman M S, Whittaker J D, Castellanos-Beltran M, Cicak K, Silva F da, DeFeo M P, Lecocq F, Sirois A, Teufel J D, Aumentado J and Simmonds R W 2014 *Phys. Rev. Lett.* **112** 123601
[55] Chen Y, Neill C, Roushan P, Leung N, Fang M, Barends R, Kelly J, Campbell B, Chen Z, Chiaro B, Dunsworth A, Jeffrey E, Megrant A, Mutus J Y, O'Malley P J J, Quintana C M, Sank D, Vainsencher A, Wenner J, White T C, Geller M R, Cleland A N and Martinis J M 2014 *Phys. Rev. Lett.* **113** 220502
[56] Müller C, Guan S, Vogt N, Cole J H and Stace T M 2018 *Phys. Rev. Lett.* **120** 213602
[57] Yin Y, Chen Y, Sank D, O'Malley P J J, White T C, Barends R, Kelly J, Lucero E, Mariantoni M, Megrant A, Neill C, Vainsencher A, Wenner J, Korotkov A N, Cleland A N and Martinis J M 2013 *Phys. Rev. Lett.* **110** 107001
[58] Forn-Díaz P, Lisenfeld J, Marcos D, García-Ripoll J J, Solano E, Harmans C J P M and Mooij J E 2010 *Phys. Rev. Lett.* **105** 237001
[59] Niemczyk T, Deppe F, Huebl H, Menzel E P, Hocke F, Schwarz M J, Garcia-Ripoll J J, Zueco D, Hummer T, Solano E, Marx A and Gross R 2010 *Nat. Phys.* **6** 772